

# Influence of wing span on the aerodynamics of wings in ground effect

Sammy Diasinos<sup>1</sup>, Tracie J Barber<sup>2</sup> and Graham Doig<sup>2</sup>

## Abstract

A computational fluid dynamics study of the influence of wing span has been conducted for an inverted wing with endplates in ground effect. Aerodynamic coefficients were determined for different spans at different ground clearances, highlighting a trend for shorter spans to delay the onset of both separation and resulting loss of negative lift. The vortices at the wing endplates were not observed to change significantly in terms of strength and size; thus, at shorter spans, their influence over a larger percentage of the wing helped the flow stay attached and reduced the severity of the adverse pressure gradient which invokes separation at greater spans. Consequently, it was shown that, compared to a large-span wing, a wing with a shorter span may have a lower lift coefficient but can operate closer to the ground before performance is adversely affected.

## Introduction

Detailed experiments by Zerihan et al. on the aerodynamics of an inverted (downforce-producing) wing in ground effect,<sup>1–5</sup> and subsequent numerical analysis of the test geometry (based on a modified NASA GA(W) LS(1)-0413),<sup>6,7</sup> have highlighted significant three-dimensional effects with regards to spanwise pressure distributions as well as vortex formation and downstream behaviour. The availability of these experimental results makes the inverted wing a good candidate for fundamental and parametric studies. However, the studied wing had a fixed aspect ratio of 4.92 (corresponding to the real-world Formula 1 wing on which it was based), and thus the influence of span on the overall performance of the wing, including the effects on susceptibility to the lift-loss phenomenon, was not established. Nor was the true two-dimensionality of flow at the semi-span evaluated. Wing span and related endplate effects are important variables when designing wind tunnel experiments to obtain quasi-two-dimensional sectional pressures and forces on highly cambered wings in ground effect,<sup>7</sup> and given that front wing regulations change regularly in open-wheel categories, the influence of span is certainly worth characterizing and understanding in greater depth.

The series of experiments and simulations conducted by Ranzenbach<sup>8</sup> and Ranzenbach and Barlow<sup>9</sup> in the mid-1990s represented the first systematic public investigation of downforce-producing wings in ground effect, and they noted that a wing would continue to increase in drag and downforce as ground clearance reduced. This trend held until very low clearances (for instance, a height-to-chord ratio  $h/c=0.097$  for a NACA4412 section), at which point the negative lift produced would reach a maximum and then drop off with continued ground proximity. They attributed this to the ‘merging’ of boundary layers between the ground and the wing, whether a moving or stationary ground was implemented.

However, from Zerihan’s study of a single-element inverted wing in ground effect, it was determined that

---

<sup>1</sup>Caterham F1, UK

<sup>2</sup>School of Mechanical and Manufacturing Engineering, The University of New South Wales, Australia

## Corresponding author:

Graham Doig, School of Mechanical and Manufacturing Engineering, The University of New South Wales, Kensington, Sydney, NSW 2052, Australia.

Email: g.doig@unsw.edu.au

this ‘downforce loss phenomenon’ is caused when a severe adverse pressure gradient on the bottom surface of the wing leads to boundary layer separation,<sup>1,5</sup> and is enhanced by factors such as wing angle of attack as well as the parameter of camber as previously identified by Ranzenbach and Barlow.<sup>9</sup>

Additionally, surface flow visualization indicated that the separation was more pronounced at the centre of the wing than at the tips. The cause of this was attributed to the main wing vortex, which forms on the bottom edge of the endplate, re-energizing the boundary layer and preventing separation from occurring near the wing tips. Simultaneously, the centre of the wing experiences a greater adverse pressure gradient due to the larger peak suction values achieved there. Based on this, the present article poses the hypothesis that, as the wing span decreases, the height at which the maximum downforce occurs will also reduce because the main wing vortex that limits the separation towards the tips will act over a greater percentage of the bottom surface.

To examine this, a computational model was used to test four additional increments of wing semi-span ( $b/c = 2, 1.6, 1.24$  and  $0.97$ ) of the original wing geometry (semi-span of  $2.46c$ ). Coordinates and dimensions of the wing and wind tunnel can be found in the original documentation for the tests.<sup>1</sup>

## Numerical method

The numerical approach used to generate the results in this note is extremely similar to those used in previous studies utilizing the same wing section.<sup>6,7</sup> The general meshing approach and choice of turbulence model have therefore been extensively validated against the original experiments of Zerihan,<sup>1</sup> and for the sake of brevity are merely summarized here.

A commercial finite-volume Reynolds-averaged Navier–Stokes solver, Fluent, was used to generate all results. This software is commonly used in the automotive and aerospace industries. An implicit, pressure-based approach was applied to obtain steady-state solutions. Although unsteady effects in scenarios featuring separation may be an important aspect, transient solutions are still rarely undertaken by racing car teams due to the excessive computational expense. Grid independence of the three-dimensional hexahedral mesh (approximately  $8 \times 10^6$  cells,  $y^+$  of approximately 1 on the wing) has previously been verified through extensive comparison to experiment.<sup>6</sup> Figure 1 shows the domain extent and an example mesh (for the original wing span). For this study, wing transition was not imposed (as it was in the original experiments) so as to eliminate it as an influence on the results – a real-world racing car wing would feature free transition and future work, considering the effect of span on this variable would be useful.

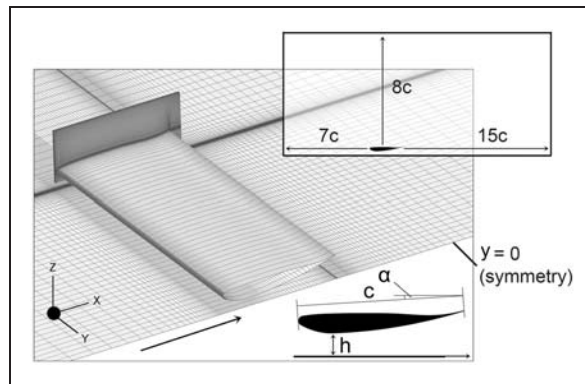


**Figure 1.** Example mesh, domain extents and relevant parameters for an inverted wing in ground effect.

The numerical model was constructed to replicate the experiments with high fidelity, and therefore the endplates were included and meshed appropriately, and the freestream flow velocity was  $30 \text{ ms}^{-1}$ , giving a Reynolds number of approximately  $4.6 \times 10^5$ . The moving ground was represented at a velocity matching the freestream, to ensure correct ground boundary representation,<sup>10</sup> and a simplified version of the original wind tunnel walls was used since the full complexity of the tunnel has previously been shown to have negligible influence on the flowfield.<sup>7</sup> Turbulent intensity was set to 0.2%, from the measured mean value. The wing was set at a reference incidence described in the literature.<sup>1</sup> Ground clearance, defined in terms of height-to-chord ratio,  $h/c$ , was measured from the chordwise point on the wing surface closest to the ground plane. An obvious omission from the computational model is the support struts which held the wing in place in the tunnel. Unfortunately, little is known about the exact geometry of these struts but it is expected that their influence on the overall flowfield was very small.<sup>1</sup>

Three common turbulence models were used for a preliminary comparison; the one-equation Spalart–Allmaras model,<sup>11</sup> the two-equation realizable  $k-\varepsilon\psi$  model,<sup>12</sup> and the shear stress transport variant of the  $k-\omega$  closure.<sup>13</sup> In well-resolved three-dimensional studies, these models perform in a relatively similar and capable fashion.<sup>7</sup> By a small margin, the realizable  $k-\varepsilon\psi$  model proved to be most capable at matching experimental results and thus was used for the study described here.

## Results

The computed lift coefficients are shown in Figure 2. Reducing the span of the wing highlights a clear relationship with the height at which the downforce loss phenomenon occurs. For the wing semi-span values

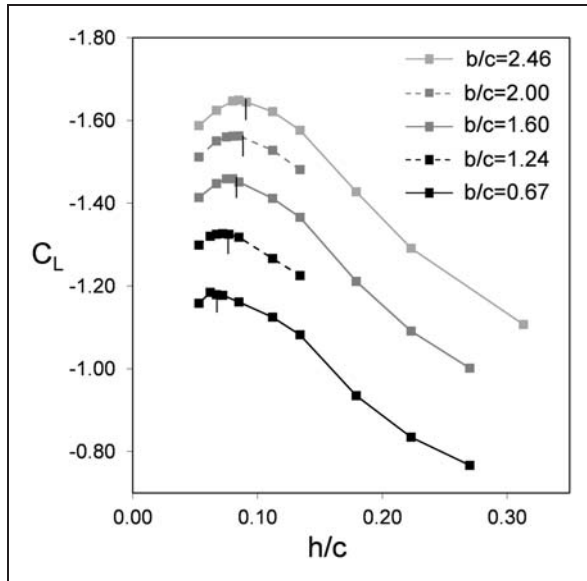


**Figure 2.** Lift coefficient versus ground clearance for various wing semi-spans.

2.00c, 1.60c, 1.24c and 0.97c, it was determined that the height-to-chord ratio at which the downforce loss phenomenon occurred was reduced to 0.080, 0.078, 0.072 and 0.062, respectively, compared to 0.085 as originally determined experimentally and numerically for the semi-span of 2.46c. To determine if the cause for this variation was caused by the main wing vortex acting over a larger portion of the wing, the spanwise extent of separation along the wing was investigated using wall shear stress as an indicator of where separation would occur – in comparison to original oil surface visualization, a value of less than 1 was deemed to be a sufficient indicator for the onset of the separated region.

Separation is more pronounced over the centre portion of the wing, while a region closer to the wing tip, where the main wing vortex has the largest influence, remains attached with a reduction in peak flow velocity and a corresponding reduction in the severity of the adverse pressure gradient. At shorter spans, the size of the vortex remains fairly constant and therefore acts over a larger portion of the wing as the span is reduced. Figure 3 highlights this effect by comparing wall shear stress contours for lower surfaces of different semi-spans at their respective ground clearances for maximum downforce (i.e. beyond which the downforce loss occurs). The results shown here indicate that the separated region is expected to form from the centre of the wing until 0.4c inboard from the endplate. This suggests that for wing semi-spans of 0.97c, 1.24c, 1.60c, 2.00c and 2.46c, the region in which the vortex acts to limit separation from occurring is approximately 40%, 31%, 25%, 20% and 16% of the span, respectively, allowing

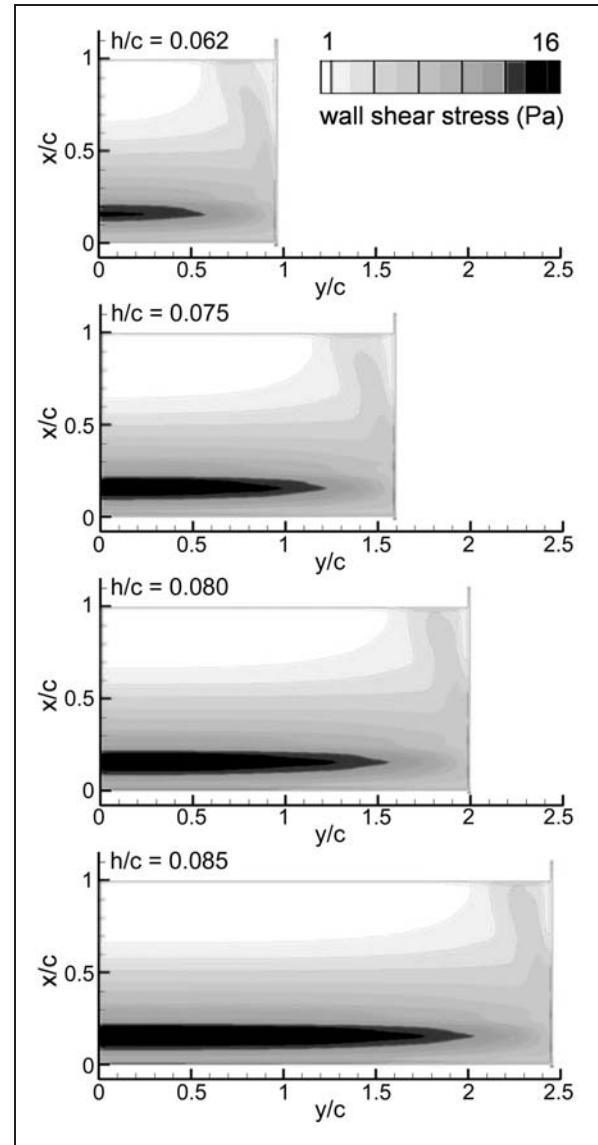


**Figure 3.** Wall shear stress for wing semi-spans at respective ground clearances for maximum downforce.

the downforce loss to occur at lower clearances for a shorter span of wing, though the overall lift coefficient is greatly reduced. The figure also re-enforces the notion that the separation point and vortex strength is essentially unchanging at the point at which the downforce loss begins; a shorter span at a ground proximity equivalent to that at which a wider span would reach its downforce peak would feature later separation in the chordwise sense.

In order for the vortex to act over what is essentially a constant area, the vortex strength would have to remain unchanged for variations in span. The main wing vortex is created by the pressure difference between the sides of the endplates, and this is dependent on the pressure difference that can be achieved by the upper and lower

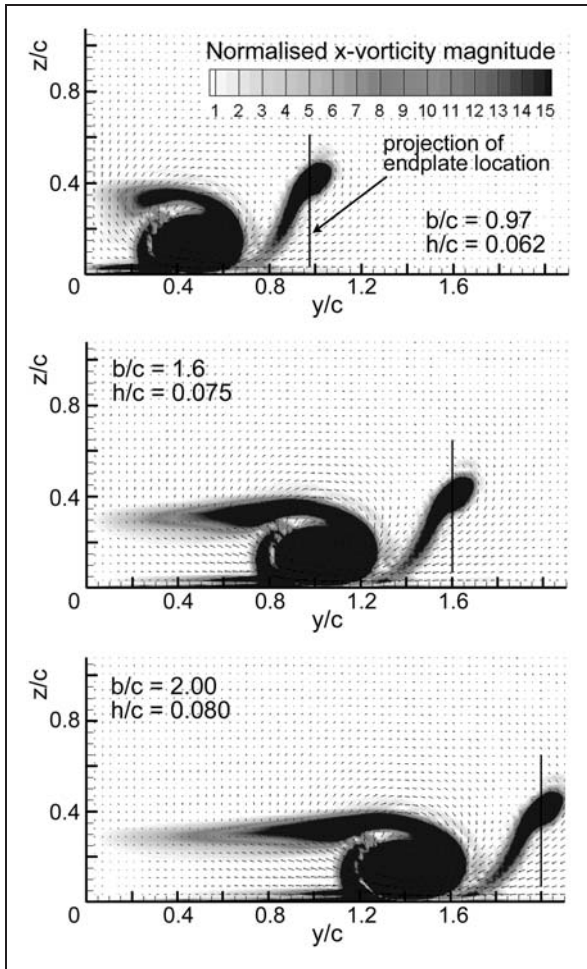


**Figure 4.** Normalized x-vorticity magnitude at a plane  $0.75c$  downstream for wing semi-spans of 0.97, 1.6 and 2 for respective ground clearances for maximum downforce.

surfaces. Vorticity plots on a plane located at  $x/c = 0.75$  downstream from the wing leading edge, shown in Figure 4, indicated that the main wing vortex had a core diameter that remains between 0.5 and 0.55 of chord at the height at which the maximum downforce is achieved for each specific span.

Spanwise pressure coefficients indicated that the most significant variation occurs at the centre of the wing ( $y/c = 0$ ), where a reduction in span results in reduced levels of suction acting on the bottom surface. This points to a coupled reason why the downforce loss phenomenon is delayed as the span is reduced, and is best explained by considering the pressure distribution over the central chord of each wing at a fixed height (Figure 5). For a given height, as the span is reduced, the minimum pressure experienced by the bottom surface also reduces as the flow trends away from a purely two-dimensional solution free of endplate effects. This results in a less-severe adverse pressure gradient, ensuring that as the span is reduced, the flow over the centre

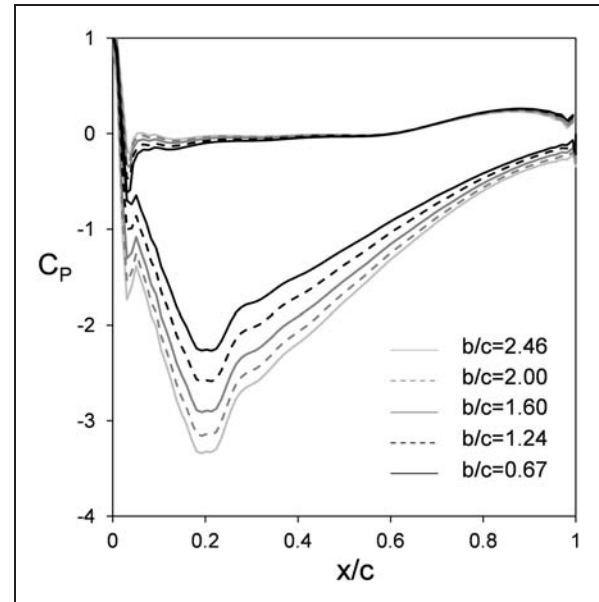


**Figure 5.** Pressure coefficient distributions for various wing semi-spans at  $h/c = 0.134$ .

portion of the bottom surface of the wing will remain attached at lower ground clearances. A certain adverse gradient is required to instigate separation, and this is almost identical for all spans for their respective ground clearances for the onset of the downforce loss phenomenon. The peak suction pressure at the maximum downforce clearance obtained for each span varies less than that obtained at a common height, ensuring that the adverse pressure gradient seen on the bottom surface of the wing is also similar, and therefore the extent of the separation is also relatively consistent.

Given that the wing vortex size remains fairly constant, and that the main variations that cause the reduced levels of downforce are due to the variation of pressure acting on the surface of the wing, it would be expected that as the wing span is reduced, the induced drag created by the formation of the main wing vortex of the wing would be of greater significance. The drag coefficients presented in Figure 6 suggest that this is the case with the shortest semi-span tested ( $b = 0.97c$ ), indicating that the maximum drag coefficient is obtained at the same height at which the maximum downforce is achieved ( $h = 0.062c$ ). At lower clearances, the wing vortex is prone to bursting and as a result, the induced drag of the wing reduces, accounting for the subsequent reductions in drag obtained at this span as the clearance is further reduced. As the span is increased, the significance of the induced drag is outweighed by the increases in the pressure drag caused by the separation from the bottom surface of the wing. For this reason, the drag coefficient for variations in  $h/c$  tends to increase for reductions in height at a more rapid rate as the span is

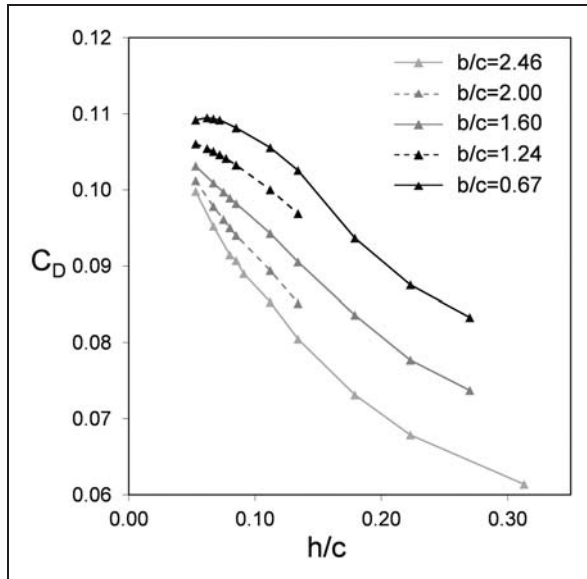


**Figure 6.** Drag coefficient versus ground clearance for various wing semi-spans.

increased and separation affects a greater percentage of the bottom surface of the wing.

## Conclusion

It has been demonstrated that reducing the span of an inverted wing with an endplate allows it to operate closer to the ground before the downforce loss phenomenon occurs. There are two related causes: the first being that the main wing vortex that prevents separation from occurring at the wing tip remains largely unchanged with variations in span, thus effectively acting over a greater portion of the wing when the span is short. Second, the shorter span wings have reduced suction on the bottom surface due to the increased three-dimensionality of the flow, and as a result, the wing can operate much closer to the ground before the pressure gradient becomes severe enough to result in large-scale separation on the bottom surface of the wing.

## Funding

This research was funded internally by the University of New South Wales.

## References

1. Zerihan J. *An investigation into the aerodynamics of wings in ground effect*. PhD Thesis, School of Engineering Sciences, University of Southampton, UK, 2001.

2. Zerihan J and Zhang X. Aerodynamics of a single element wing in ground effect. *J Aircr* 2000; 37(6): 1058–1064.
3. Zerihan J and Zhang X. Aerodynamics of gurney flaps on a wing in ground effect. *AIAA J* 2001; 39(5): 772–780.
4. Zhang X and Zerihan J. Off-surface aerodynamic measurements of a wing in ground effect. *J Aircr* 2003; 40(4): 716–725.
5. Zhang X and Zerihan J. Edge vortices of a double element wing in ground effect. *J Aircr* 2004; 41(5): 1127–1137.
6. Doig G, Barber T and Neely A. The influence of compressibility on the aerodynamics of an inverted wing in ground effect. *ASME J Fluids Eng* 2011; 133(6): 1–12.
7. Doig G and Barber T. Considerations for numerical modeling of low aspect ratio inverted wings in ground effect. *AIAA J* 2011; 49(10): 2330–2333.
8. Ranzenbach R. Cambered airfoil in ground effect –wind tunnel and road conditions. In: *Proceedings of the 13th AIAA applied aerodynamics conference*, San Diego, USA, 19–22 June 1995, pp.1208–1215.
9. Ranzenbach R and Barlow J. Cambered aerofoil in ground effect - an experimental and computational study. In: *SAE international congress & exposition*, February 26–29 February 1996, Detroit, MI, SAE paper 960909.
10. Barber TJ, Leonardi E and Archer RD. Causes for discrepancies in ground effect analyses. *Aeronaut J* 2002; 106(1066): 653–657.
11. Spalart P and Allmaras S. A one-equation turbulence model for aerodynamic flows. AIAA paper 92-0439, 1992.
12. Shih TH, Liou WW, Shabbir A, Yang Z and Zhu J. A new  $k-\epsilon$  eddy-viscosity model for high Reynolds number turbulent flows-model development and validation. *Comput Fluids* 1995; 24(3): 227–238.
13. Menter FR. Two-equation eddy-viscosity turbulence models for engineering applications. *AIAA J* 1994; 32(8): 269–289.

## Appendix

### Notation

$b$	semi-span
$c$	chord
$C_D$	drag coefficient
$C_L$	negative lift (downforce) coefficient
$c_p$	pressure coefficient
$h$	height above the ground plane
$\alpha$	wing angle of incidence